Atomistic simulation of MgO nanowires subject to electromagnetic wave

2010 Modelling Simul. Mater. Sci. Eng. 18 085010

(http://iopscience.iop.org/0965-0393/18/8/085010)

Modelling Simul. Mater. Sci. Eng. **18** (2010) 085010 (15pp) doi:10.1088/0965-0393/18/8/085010

Atomistic simulation of MgO nanowires subject to electromagnetic wave

Xianqiao Wang and James D Lee

Department of Mechanical and Aerospace Engineering, The George Washington University, Washington, DC 20052, USA

Received 20 July 2010, in final form 4 November 2010
Published 25 November 2010
Online at stacks.iop.org/MSMSE/18/085010

Abstract

This work is concerned with the application of atomistic field theory (AFT) in modeling and simulation of polarizable materials under an electromagnetic (EM) field. AFT enables us to express an atomic scale local property of a multi-element crystalline (which has more than one kind of atom in the unit cell) system in terms of the distortions of lattice cells and the rearrangement of atoms within the lattice cell, thereby making AFT suitable to fully reproduce both acoustic and optical branches in phonon dispersion relations. Due to the applied EM field, the inhomogeneous motions of discrete atoms in the polarizable crystal give rise to the rearrangement of microstructure and polarization. The AFT and its corresponding finite element implementation are briefly introduced. Single-crystal MgO nanowires under an EM field is modeled and simulated. The numerical results have demonstrated that AFT can serve as a tool to analyze the electromagnetic phenomena of multi-element crystal materials at micro/nano-level within a field framework.

(Some figures in this article are in colour only in the electronic version)

1. Introduction

Optical phonon branches exist in all crystals that have more than one atom per primitive unit cell. Under an electromagnetic field it is the optical modes that are excited. Optics is a phenomenon that necessitates the presence of an electromagnetic field. While classical continuum theory is the long acoustic wave limit, lattice dynamics analysis has shown that micromorphic theory [1–3] yields phonon dispersion relation similar to those from atomistic calculations and experimental measurements [4, 5]. It provides up to 12 phonon dispersion relations, including three acoustic and nine optical branches. The optical phonons in micromorphic theory describe the internal displacement patterns within the microstructure of material particles consistent with the internal atomic displacements in the optical modes.

The past few decades have seen the explosive growth of multiscale modeling approaches for linking atomistic with macroscopic models. Among them are the coupled length scale

method [6], the bridging scale method [7], the bridging domain method [8], the mathematical homogenization theory [9], the atomistic-to-continuum method [10] and so forth. Despite different treatments in the coupling strategy, these methods share basic principles, and typically have three components: a finite element (FE) representation for continuum subdomains where the deformation field is smooth and homogeneous; a molecular dynamics description for atomistic subdomains in which bond breaking is expected; a strategy to couple these two representations. Differences in the available coupling methods are the specifics of the coupling strategies, which have been extensively reviewed in [11, 12]. Another typical popular bottom-up approach is the quasicontinuum method [13]. The chief objective of the method is to coarsen an atomistic description systematically by the judicious introduction of kinematic constraints. These kinematic constraints are selected and designed to preserve full atomistic resolution where required and to treat collectively large numbers of atoms in regions where the deformation field varies slightly on the scale of the lattice.

It is also worth mentioning that micromorphic theories are the logical extensions of the classical field theories for the applications in microscopic space and short time scales. The fundamental difference between the microcontinuum field theory and the classical continuum mechanics is that the former are continuum models embedded with microstructure for the purpose of capturing the microscopic motion and deformation. Micromorphic theory treats a material as a continuous collection of deformable particles, each particle possessing a finite size and inner structure. Chen *et al* [4] examined the physical foundation of those microcontinuum theories from the viewpoint of phonon dispersion relations, and concluded that the applicability of those microcontinuum theories is limited because of the continuum assumption of the microstructure. Motivated by the applicability and limitation of microcontinuum theories as well as by a bottom-up formalism of linking atomistic model to continuum descriptions by Irvine and Kirkwood [14] and Hardy [15], atomistic field theory (AFT) has been constructed by Chen and her coworkers [16–21] for concurrent atomistic/continuum modeling of materials/systems. Continuous local densities of fundamental physical quantities in atomistic systems are derived. By decomposing atomic motion/deformation into homogeneous lattice motion/deformation and inhomogeneous internal atomic motion/deformation, and also decomposing momentum flux and heat flux into homogeneous and inhomogeneous parts, field description of conservation laws at atomic scale has been formulated. Subsequently, a field representation of atomistic system is obtained, leading naturally to an atomistic/continuum theory, in which a material is viewed as a continuous collection of lattice points, while embedded within each lattice point is a group of discrete atoms. In AFT, the lattice deformation is homogenous and continuous, but the internal deformation is inhomogeneous.

This paper is concerned with the application of AFT in the simulation of a rocksalt crystal MgO under an electromagnetic wave. Following this introduction, the atomistic formulation of AFT will be briefly introduced in section 2 and the FE implementation will be developed in section 3. In section 4, we will present the response of MgO nanowires under an EM wave to demonstrate the characteristics and the advantages of AFT. We conclude this paper with a brief summary and discussion in section 5.

2. Atomistic field theory

To provide the background for the subsequent developments, we briefly review the AFT constructed by Chen and her coworkers [16–21] and its corresponding numerical algorithm by Lee *et al* [18, 19]. In contrast to the classical statistical mechanics approaches or the existing formalisms that link unit-cell variables to continuum field variables, AFT views a crystalline material as a continuous collection of lattice cells and a group of discrete and distinct atoms

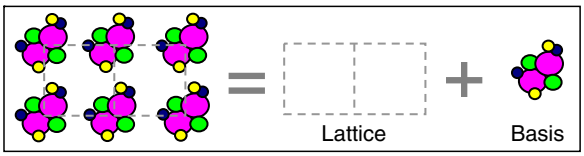

Figure 1. Atomistic view of the crystal structure.

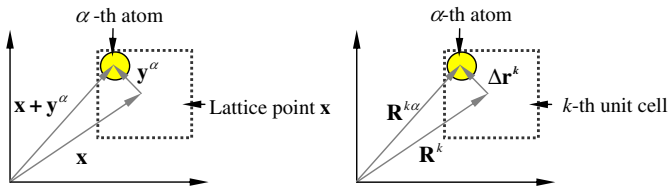

Figure 2. Relation between physical space and phase space descriptions.

situated within each lattice cell as shown in figure 1. Thus, a more general link, shown in figure 2, between any phase space function $\boldsymbol{A}(\boldsymbol{r}, \boldsymbol{p})$ and the corresponding local density function $\boldsymbol{a}(\boldsymbol{x}, \boldsymbol{y}^\alpha, t)$ was developed by Chen [9] as

$$\boldsymbol{a}(\boldsymbol{x}, \boldsymbol{y}^\alpha, t) = \sum_{k=1}^{N_l} \sum_{\xi=1}^{N_a} \boldsymbol{A}(\boldsymbol{r}, \boldsymbol{p}) \delta(\boldsymbol{R}^k - \boldsymbol{x}) \tilde{\delta}(\Delta \boldsymbol{r}^{k\xi} - \boldsymbol{y}^\alpha) \qquad (\alpha = 1, 2, 3, \ldots, N_a), \tag{1}$$

where $\boldsymbol{r}$ and $\boldsymbol{p}$ are the positions and momenta of atoms in the phase space, respectively, the superscript $k\xi$ refers to the ξth atom in the kth unit cell, $\boldsymbol{R}^k$ is the position of the mass center of the kth unit cell, $\Delta \boldsymbol{r}^{k\xi}$ is the atomic position of the ξth atom relative to the mass center of the kth unit cell, $\boldsymbol{x}$ and $\boldsymbol{y}^\alpha$ are the corresponding physical space counterparts of $\boldsymbol{R}^k$ and $\Delta \boldsymbol{r}^{k\alpha}$, N_l is the total number of unit cells in the system and N_a is the number of atoms in a unit cell. The first delta function in equation is a localization function. It can be a Dirac δ-function [14] or a distribution function [15]. The field descriptions of the conservation equations and the constitutive relations have been proved to be independent of the choices of the localization function [22]. The second delta function in equation is the Kronecker delta, which identifies $\boldsymbol{y}^\alpha$ to $\Delta \boldsymbol{r}^{k\alpha}$.

The time evolution of any physical quantity in the AFT can be expressed as

$$\begin{aligned} \left.\frac{\partial \boldsymbol{a}(\boldsymbol{x}, \boldsymbol{y}^\alpha, t)}{\partial t}\right|_{\boldsymbol{x}, \boldsymbol{y}^\alpha} &= \textstyle\sum_{k=1}^{N_l} \sum_{\xi=1}^{N_a} \dot{\boldsymbol{A}}(\boldsymbol{r}, \boldsymbol{p}) \delta(\boldsymbol{R}^k - \boldsymbol{x}) \tilde{\delta}(\Delta \boldsymbol{r}^{k\xi} - \boldsymbol{y}^\alpha) \\ &\quad - \nabla_{\boldsymbol{x}} \cdot \textstyle\sum_{k=1}^{N_l} \sum_{\xi=1}^{N_a} \boldsymbol{V}^k \otimes \boldsymbol{A}(\boldsymbol{r}, \boldsymbol{p}) \delta(\boldsymbol{R}^k - \boldsymbol{x}) \tilde{\delta}(\Delta \boldsymbol{r}^{k\xi} - \boldsymbol{y}^\alpha) \\ &\quad - \nabla_{\boldsymbol{y}^\alpha} \cdot \textstyle\sum_{k=1}^{N_l} \sum_{\xi=1}^{N_a} \Delta \boldsymbol{v}^{k\xi} \otimes \boldsymbol{A}(\boldsymbol{r}, \boldsymbol{p}) \delta(\boldsymbol{R}^k - \boldsymbol{x}) \tilde{\delta}(\Delta \boldsymbol{r}^{k\xi} - \boldsymbol{y}^\alpha). \end{aligned} \tag{2}$$

When $\boldsymbol{a}(\boldsymbol{x}, \boldsymbol{y}^\alpha, t)$ is the local density of a conserved quantity, equation (2) represents the corresponding balance law.

By means of equation (1), the local density quantities, such as mass density ρ^α, linear momentum density $\rho^\alpha(\boldsymbol{v} + \Delta \boldsymbol{v}^\alpha)$, internal energy density $\rho^\alpha e^\alpha$ and temperature T^α, are defined as

$$\rho^\alpha \equiv \sum_{k=1}^{N_l} \sum_{\xi=1}^{N_a} m^\xi \delta(\boldsymbol{R}^k - \boldsymbol{x}) \tilde{\delta}(\Delta \boldsymbol{r}^{k\xi} - \boldsymbol{y}^\alpha), \tag{3}$$

$$\rho^\alpha(\boldsymbol{v} + \Delta \boldsymbol{v}^\alpha) \equiv \sum_{k=1}^{N_l} \sum_{\xi=1}^{N_a} m^\xi (\boldsymbol{V}^k + \Delta \boldsymbol{v}^{k\xi}) \delta(\boldsymbol{R}^k - \boldsymbol{x}) \tilde{\delta}(\Delta \boldsymbol{r}^{k\xi} - \boldsymbol{y}^\alpha), \tag{4}$$

$$\rho^\alpha e^\alpha \equiv \sum_{k=1}^{N_l}\sum_{\xi=1}^{N_a}\left[\frac{1}{2}m^\xi(\tilde{\boldsymbol{V}}^{k\xi})^2 + U^{k\xi}\right]\delta(\boldsymbol{R}^k - \boldsymbol{x})\tilde{\delta}(\Delta\boldsymbol{r}^{k\xi} - \boldsymbol{y}^\alpha), \tag{5}$$

$$T^\alpha \equiv \frac{\Delta V}{3k_\mathrm{B}}\sum_{k=1}^{N_l}\sum_{\xi=1}^{N_a} m^\xi(\tilde{\boldsymbol{V}}^{k\xi})^2\delta(\boldsymbol{R}^k - \boldsymbol{x})\tilde{\delta}(\Delta\boldsymbol{r}^{k\xi} - \boldsymbol{y}^\alpha), \tag{6}$$

where $\tilde{\boldsymbol{V}}^{k\xi} \equiv \boldsymbol{V}^{k\xi} - (\boldsymbol{v} + \Delta\boldsymbol{v}^\xi)$ is the difference between phase space velocity and local physical space velocity, $\boldsymbol{v}$ is the velocity of the mass centre of a unit cell in the local physical space, $\boldsymbol{V}^k$ is the velocity of the mass centre of the kth unit cell in the phase space, $\Delta\boldsymbol{v}^\alpha$ is the velocity of the αth atom relative to the centre of the unit cell in the local physical space, $\Delta\boldsymbol{v}^{k\xi}$ is the velocity of the $k\xi$th atom relative to the centre of the kth unit cell in the phase space, $U^{k\xi}$ is the potential energy of the $k\xi$th atom, k_B is the Boltzmann constant and ΔV is the volume of a unit cell.

Following equation (2), as exact consequences of Newton's second laws, we have the time evolution of conserved quantities, namely, mass, linear and angular momenta and energy, as [17]

$$\frac{\mathrm{d}\rho^\alpha}{\mathrm{d}t} + \rho^\alpha\nabla_{\boldsymbol{x}}\cdot\boldsymbol{v} + \rho^\alpha\nabla_{\boldsymbol{y}^\alpha}\cdot\Delta\boldsymbol{v}^\alpha = 0, \tag{7}$$

$$\rho^\alpha\frac{\mathrm{d}}{\mathrm{d}t}(\boldsymbol{v} + \Delta\boldsymbol{v}^\alpha) = \nabla_{\boldsymbol{x}}\cdot\boldsymbol{t}^\alpha + \nabla_{\boldsymbol{y}^\alpha}\cdot\tau^\alpha + \boldsymbol{\varphi}^\alpha, \tag{8}$$

$$\boldsymbol{t}^\alpha + \boldsymbol{\tau}^\alpha = (\boldsymbol{t}^\alpha + \boldsymbol{\tau}^\alpha)^\mathrm{T}, \tag{9}$$

$$\rho^\alpha\frac{\mathrm{d}e^\alpha}{\mathrm{d}t} + \nabla_{\boldsymbol{x}}\cdot(-\boldsymbol{q}^\alpha) + \nabla_{\boldsymbol{y}^\alpha}\cdot(-\boldsymbol{j}^\alpha) = \boldsymbol{t}^\alpha : \nabla_{\boldsymbol{x}}(\boldsymbol{v} + \Delta\boldsymbol{v}^\alpha) + \tau^\alpha : \nabla_{\boldsymbol{y}^\alpha}(\boldsymbol{v} + \Delta\boldsymbol{v}^\alpha) + h^\alpha, \tag{10}$$

where $\boldsymbol{\varphi}^\alpha$ is the external force density; $\boldsymbol{t}^\alpha$ and $\boldsymbol{\tau}^\alpha$ are the homogeneous and inhomogeneous parts of the atomic stress tensor, which further consist of a kinetic part that is related to temperature, and a potential part that is related to the interatomic force density; $\boldsymbol{q}^\alpha$ and $\boldsymbol{j}^\alpha$ are the homogenous and inhomogeneous parts of heat flux, which also consist of kinetic and potential parts and h^α is the heat source.

For a single-element atomic system, Cheung and Yip [23] gave the following definitions for kinetic stresses $\hat{t}_{ij}$ and temperature $\hat{T}$:

$$\hat{t}_{ij} = -\sum_{l=1}^{N} m\tilde{v}_i^l\tilde{v}_j^l/\hat{V}, \qquad 3Nk_\mathrm{B}\hat{T} = \sum_{l=1}^{N} m\tilde{v}_i^l\tilde{v}_i^l, \tag{11}$$

where $\hat{V}$ is the volume that the N atoms occupy and $\tilde{v}_i^l$ is the difference velocity of the ith component between instantaneous velocity and average velocity of the lth atom. Consistent with Cheung and Yip, for multi-element atomic system, we have

$$\begin{aligned}
\boldsymbol{t}^\alpha_\mathrm{kin} &= -m^\alpha\tilde{\boldsymbol{v}}\otimes(\tilde{\boldsymbol{v}} + \Delta\tilde{\boldsymbol{v}}^\alpha)/\Delta V,\\
\boldsymbol{\tau}^\alpha_\mathrm{kin} &= -m^\alpha\Delta\tilde{\boldsymbol{v}}^\alpha\otimes(\tilde{\boldsymbol{v}} + \Delta\tilde{\boldsymbol{v}}^\alpha)/\Delta V,\\
3k_\mathrm{B}T^\alpha &= m^\alpha(\tilde{\boldsymbol{v}} + \Delta\tilde{\boldsymbol{v}}^\alpha)\cdot(\tilde{\boldsymbol{v}} + \Delta\tilde{\boldsymbol{v}}^\alpha).
\end{aligned} \tag{12}$$

It is seen that $\boldsymbol{t}^\alpha_\mathrm{kin} + \boldsymbol{\tau}^\alpha_\mathrm{kin} = -m^\alpha(\tilde{\boldsymbol{v}} + \Delta\tilde{\boldsymbol{v}}^\alpha)\otimes(\tilde{\boldsymbol{v}} + \Delta\tilde{\boldsymbol{v}}^\alpha)/\Delta V$ is symmetric; but neither $\boldsymbol{t}^\alpha_\mathrm{kin}$ nor $\boldsymbol{\tau}^\alpha_\mathrm{kin}$ is symmetric. At temperature higher than Debye temperature and within the harmonic approximation, all modes have the same energy [24]. This implies

$$(N_a - 1)m\tilde{\boldsymbol{v}}\cdot\tilde{\boldsymbol{v}} = \sum_{\alpha=1}^{N_a} m^\alpha\Delta\tilde{\boldsymbol{v}}^\alpha\cdot\Delta\tilde{\boldsymbol{v}}^\alpha, \tag{13}$$

where $m = \sum_{\alpha=1}^{N_a} m^\alpha$ is the total mass of a unit cell. Equation (12) implies

$$t^\alpha_{ij\,(\mathrm{kin})} = -\frac{\lambda^\alpha k_\mathrm{B} T \delta_{ij}}{\Delta V}, \qquad \tau^\alpha_{ij\,(\mathrm{kin})} = -\frac{(1-\lambda^\alpha) k_\mathrm{B} T \delta_{ij}}{\Delta V}, \tag{14}$$

where $\lambda^\alpha = m^\alpha/m$. Definition of temperature at nanoscale is still a debating issue. Here, we follow the classical way to define temperature as a measure of thermal energy over a finite duration and over a unit cell. Thus, we have $T^\alpha = T(\boldsymbol{x}, t)$ and $\nabla_{y^\alpha} \cdot \boldsymbol{\tau}^\alpha_{\mathrm{kin}} = 0$.

Following the definition of homogeneous part $\boldsymbol{t}^\alpha_{\mathrm{pot}}$ and inhomogeneous part $\boldsymbol{\tau}^\alpha_{\mathrm{pot}}$ of potential stresses

$$\boldsymbol{t}^\alpha_{\mathrm{pot}} = -\frac{1}{2} \sum_{k,l=1}^{N_l} \sum_{\xi,\eta=1}^{N_a} (\boldsymbol{R}^k - \boldsymbol{R}^l) \otimes \boldsymbol{F}^{k\xi} B(k, \xi, l, \eta, \boldsymbol{x}, \boldsymbol{y}^\alpha), \tag{15}$$

$$\boldsymbol{\tau}^\alpha_{\mathrm{pot}} = -\frac{1}{2} \sum_{k,l=1}^{N_l} \sum_{\xi,\eta=1}^{N_a} (\Delta \boldsymbol{r}^{k\xi} - \Delta \boldsymbol{r}^{l\eta}) \otimes \boldsymbol{F}^{k\xi} B(k, \xi, l, \eta, \boldsymbol{x}, \boldsymbol{y}^\alpha) \tag{16}$$

where $\Delta\tilde{\boldsymbol{v}}^{k\xi} = \Delta \boldsymbol{v}^{k\xi} - \Delta \boldsymbol{v}^{\xi}$; $\tilde{\boldsymbol{V}}^{k\xi} = \boldsymbol{V}^{k\xi} - (\boldsymbol{v} + \Delta \boldsymbol{v}^{\xi})$; $\boldsymbol{F}^{k\xi}$ is the interatomic force acting on the $k\xi$ the atom and $B(k, \xi, l, \eta, \boldsymbol{x}, \boldsymbol{y}^\alpha)$ is defined as

$$B(k, \xi, l, \eta, \boldsymbol{x}, \boldsymbol{y}^\alpha) = \int_0^1 \delta(\boldsymbol{R}^k \lambda + \boldsymbol{R}^l (1-\lambda) - \boldsymbol{x}) \tilde{\delta}(\Delta \boldsymbol{r}^{k\xi} \lambda + \Delta \boldsymbol{r}^{l\eta} (1-\lambda) - \boldsymbol{y}^\alpha)\, \mathrm{d}\lambda. \tag{17}$$

One has

$$\nabla_{\boldsymbol{x}} \cdot \boldsymbol{t}^\alpha_{\mathrm{pot}} + \nabla_{y^\alpha} \cdot \boldsymbol{\tau}^\alpha_{\mathrm{pot}} = \boldsymbol{f}^\alpha. \tag{18}$$

Substituting the above relationships between the kinetic stress and temperature as well as that between the potential stress and the interatomic force density [18, 19] into equation (8), we obtain

$$\rho^\alpha \ddot{\boldsymbol{u}}^\alpha(\boldsymbol{x}, t) = -\frac{\lambda^\alpha k_\mathrm{B} \nabla T(\boldsymbol{x}, t)}{\Delta V} + \boldsymbol{f}^\alpha(\boldsymbol{x}, t) + \boldsymbol{\varphi}^\alpha(\boldsymbol{x}, t), \tag{19}$$

where $\dot{\boldsymbol{u}}^\alpha(\boldsymbol{x}, t) = \boldsymbol{v} + \Delta \boldsymbol{v}^\alpha$, $\ddot{\boldsymbol{u}}^\alpha(\boldsymbol{x}, t) = \mathrm{d}(\boldsymbol{v} + \Delta \boldsymbol{v}^\alpha)/\mathrm{d}t$, $\boldsymbol{f}^\alpha(\boldsymbol{x}, t)$ is the interatomic force density acting on the αth atom, $\boldsymbol{\varphi}^\alpha(\boldsymbol{x}, t)$ is the external force density acting on the αth atom, $\lambda^\alpha = m^\alpha/m$, and $m = \sum_{\alpha=1}^{N_a} m^\alpha$.

The smallest allowable physical volume in AFT is the volume of a unit cell. The mass density of the αth atom at $\boldsymbol{x}$ is thus

$$\rho^\alpha(\boldsymbol{x}, t) = \frac{m^\alpha}{\Delta V(\boldsymbol{x}, t)}, \tag{20}$$

where m^α is the mass of the αth atom. Using the atomic mass m^α as a material constant and considering that the volume of the unit cell ΔV varies during the deformation, the conservation law of mass will be automatically satisfied. Equation (20) can thus replace the traditional conservation law of mass. For systems with a given temperature field, then the relevant governing equations are just the balance law for linear momentum, i.e.

$$m^\alpha \ddot{\boldsymbol{u}}^\alpha(\boldsymbol{x}, t) = \boldsymbol{F}^\alpha_{\mathrm{t}}(\boldsymbol{x}, t) + \boldsymbol{F}^\alpha(\boldsymbol{x}, t) + \boldsymbol{F}^\alpha_{\mathrm{ext}}(\boldsymbol{x}, t), \tag{21}$$

where $\boldsymbol{F}^\alpha(\boldsymbol{x}, t)$ is the interatomic force, $\boldsymbol{F}^\alpha_t(\boldsymbol{x}, t)$ is the force due to temperature and $\boldsymbol{F}^\alpha_{\mathrm{ext}}(\boldsymbol{x}, t)$ is the force due to external fields. Here $\boldsymbol{F}^\alpha_{\mathrm{ext}}(\boldsymbol{x}, t)$ is considered as the Lorentz force [25]

$$\boldsymbol{F}^\alpha_{\mathrm{ext}} = q^\alpha(\boldsymbol{E} + \boldsymbol{v}^\alpha \times \boldsymbol{B}/c), \tag{22}$$

where q^α is the charge of the αth atom, c is the speed of light, $\boldsymbol{E}$ is the electric field, $\boldsymbol{B}$ is the magnetic flux density and $\boldsymbol{v}^\alpha$ is the velocity of the αth atom.

The existence of superscript α in equation (21) implies that the atomic information is naturally built in AFT, thereby eliminating the mismatch of phonon descriptions in atomic and continuum regions. Therefore AFT is inherently suitable for multi-element crystals, which is quite different from the classical continuum field theory and many other multiscale theories.

Define $\boldsymbol{F}^{\xi\eta}[\boldsymbol{u}^{\xi}, \boldsymbol{u}^{\eta}]$ as the interatomic force acting on an atom whose type and position are indicated by ξ and $\boldsymbol{u}^{\xi}$, respectively [19]:

$$\boldsymbol{F}^{\xi\eta}[\boldsymbol{u}^{\xi}, \boldsymbol{u}^{\eta}] = -\frac{1}{2}\left(\frac{\partial U^{\xi\eta}}{\partial \boldsymbol{u}^{\xi}} - \frac{\partial U^{\xi\eta}}{\partial \boldsymbol{u}^{\eta}}\right) = \frac{1}{2}(\boldsymbol{F}^{\xi\eta} - \boldsymbol{F}^{\eta\xi}), \tag{23}$$

where $U^{\xi\eta}$ is the interatomic potential between the ξth atom and ηth atom.

For material systems that involve pair atomic interactions, the interatomic force can $\boldsymbol{F}^{\alpha}(\boldsymbol{x}, t)$ be expressed as

$$\boldsymbol{F}^{\alpha}(\boldsymbol{x}, t) = \int_{\Omega(\boldsymbol{x}', t)} \frac{1}{\Delta V(\boldsymbol{x}', t)} \sum_{\beta=1}^{N_a} \boldsymbol{F}^{\alpha\beta}[\boldsymbol{u}^{\alpha}(\boldsymbol{x}, t), \boldsymbol{u}^{\beta}(\boldsymbol{x}', t)]\, \mathrm{d}\Omega(\boldsymbol{x}', t), \tag{24}$$

where $\Omega(\boldsymbol{x}', t)$ is the domain associated with the material point $\boldsymbol{x}'$ and $\Delta V(\boldsymbol{x}', t)$ is the volume of the unit cell located at $\boldsymbol{x}'$. It is noted that, in equation (24), full-blown nonlocality and atom-based constitutive relation are automatically rooted in the force calculation. Equations (20), (21) and (24) are invoked to solve the atomic displacement field, and consequently, atomic-scale properties.

3. FE implementation

In order to solve the above-mentioned material system efficiently and accurately, following the work done by Eidel and Stukowski [26], and Knap and Ortiz [27], we adopt two approximations. The first one is a kinematic constraint aiming at the reduction of degrees of freedom by virtue of shape functions in the FE method. The second one regards to the calculation of nodal forces in clusters with a specified summation rules. This cluster summation rules are taken as a compromise between numerical accuracy and computational efficiency [26, 27].

The essence of the numerical approach is to reduce the degrees of freedom by the kinematic constraint. Some judiciously selected unit cells, called representative unit cells or rep-cells, retain their independent degrees of freedom. Each node in the FE mesh is a rep-cell. The nodal displacements together with shape functions are employed to determine a displacement field, in other words, all other unit cells are forced to follow the motion of the nodes—this is what we called 'kinematic constraint', which is the practise used in every FE analysis. The continuous displacement filed $\boldsymbol{u}^{\alpha}(\boldsymbol{x})$ is approximated through interpolation with its nodal values $\boldsymbol{U}_I^{\alpha}$ as

$$\boldsymbol{u}^{\alpha}(\boldsymbol{x}) = \sum_{I=1}^{N_d} \Phi_I(\boldsymbol{x}) \boldsymbol{U}_I^{\alpha}, \tag{25}$$

where $\Phi_I(\boldsymbol{x})$ is the shape function and N_d is the number of nodes in each element. Following the standard procedure of the Galerkin method, the weak form of equation (21) can be written as

$$\int_{\Omega} \frac{1}{\Delta V(\boldsymbol{x})} \sum_{\alpha=1}^{N_a} \{m^{\alpha}\, \ddot{\boldsymbol{u}}^{\alpha} - \boldsymbol{F}^{\alpha} - \boldsymbol{F}_{\mathrm{ext}}^{\alpha} - \boldsymbol{F}_{t}^{\alpha}\} \cdot \delta \boldsymbol{u}^{\alpha}\, \mathrm{d}\Omega = 0, \tag{26}$$

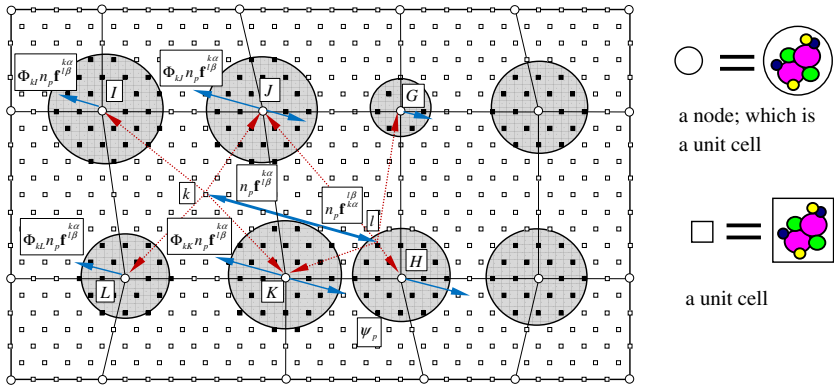

Figure 3. Schematic picture of the AFT model with force distributions.

i.e.

$$\int_{\Omega(\boldsymbol{x})} \frac{1}{\Delta V(\boldsymbol{x})} m^{\alpha} \Phi_J \Phi_I \ddot{U}_I^{\alpha} \, \mathrm{d}\Omega(\boldsymbol{x}) - \int_{\Omega(\boldsymbol{x})} \frac{1}{\Delta V(\boldsymbol{x})} \Phi_J \times \sum_{\beta=1}^{N_a} \int_{\Omega(\boldsymbol{x}')} \frac{1}{\Delta V(\boldsymbol{x}')} \boldsymbol{F}^{\alpha\beta}[\Phi_I \boldsymbol{U}_I^{\alpha}, \Phi_K(\boldsymbol{x}') \boldsymbol{U}_K^{\beta}] \mathrm{d}\Omega(\boldsymbol{x}') \, \mathrm{d}\Omega(\boldsymbol{x}) - \int_{\Omega(\boldsymbol{x})} \frac{1}{\Delta V(\boldsymbol{x})} (\boldsymbol{F}_t^{\alpha} + \boldsymbol{F}_{\mathrm{ext}}^{\alpha}) \Phi_J \, \mathrm{d}\Omega(\boldsymbol{x}) = 0. \tag{27}$$

Then the matrix form of equation (27) can be obtained as

$$\tilde{\boldsymbol{M}}_{IJ} \ddot{\boldsymbol{U}}_I^{\alpha} = \tilde{\boldsymbol{F}}_J^{\alpha} + \tilde{\boldsymbol{F}}_{\mathrm{t}J}^{\alpha} + \tilde{\boldsymbol{F}}_{\mathrm{ext}J}^{\alpha}, \tag{28}$$

where

$$\tilde{\boldsymbol{M}}_{IJ} = \int_{\Omega(\boldsymbol{x})} \frac{1}{\Delta V(\boldsymbol{x})} m^{\alpha} \Phi_J \Phi_I \, \mathrm{d}\Omega(\boldsymbol{x}), \tag{29}$$

$$\tilde{\boldsymbol{F}}_J^{\alpha} = \int_{\Omega(\boldsymbol{x})} \frac{1}{\Delta V(\boldsymbol{x})} \Phi_J \sum_{\beta=1}^{N_a} \int_{\Omega(\boldsymbol{x}')} \frac{1}{\Delta V(\boldsymbol{x}')} \boldsymbol{F}^{\alpha\beta}[\Phi_I \boldsymbol{U}_I^{\alpha}, \Phi_K(\boldsymbol{x}') \boldsymbol{U}_K^{\beta}] \, \mathrm{d}\Omega(\boldsymbol{x}') \, \mathrm{d}\Omega(\boldsymbol{x}), \tag{30}$$

$$\tilde{\boldsymbol{F}}_{\mathrm{t}J}^{\alpha} = \int_{\Omega(\boldsymbol{x})} \frac{1}{\Delta V(\boldsymbol{x})} \boldsymbol{F}_{\mathrm{t}}^{\alpha} \Phi_J \, \mathrm{d}\Omega(\boldsymbol{x}), \tag{31}$$

$$\tilde{\boldsymbol{F}}_{\mathrm{ext}J}^{\alpha} = \int_{\Omega(\boldsymbol{x})} \frac{1}{\Delta V(\boldsymbol{x})} \boldsymbol{F}_{\mathrm{ext}}^{\alpha} \Phi_J \, \mathrm{d}\Omega(\boldsymbol{x}). \tag{32}$$

All integrals in equations (29), (30), (31) and (32) are normally carried out by numerical quadrature. In figure 3, it is seen that around each node (an open circle), say the kth node, there is a cluster (a shaded area), named ψ_k. From now on, force calculation is no longer performed at all unit cells in the entire system but in all clusters. A representative unit cell (a black solid square) is the one within one of $\psi_{I_\mathrm{p}} = \{l : |\boldsymbol{X}_l - \boldsymbol{X}_{I_\mathrm{p}}| \leqslant R_{I_\mathrm{p}}\}$. Note that there is no overlapping of clusters. $\boldsymbol{X}_l$ is the position of the lth unit cell and R_{I_p} is the radius of the

Table 1. Short-range interaction parameters for different pairs in MgO.

Species	Species	A (eV)	ρ (Å)	C (eV(Å)^6)
O^{2-}	O^{2-}	9547.96	0.2192	32.0
Mg^{2+}	O^{2-}	1284.38	0.2997	0.00
Mg^{2+}	Mg^{2+}	0.00000	0.0000	0.00

cluster ψ_{I_p} centered at the I_pth node. We postulate that the cluster summation rule reads

$$\tilde{\boldsymbol{F}}_J^\alpha = \int_{\Omega(\boldsymbol{x})} \frac{1}{\Delta V(\boldsymbol{x})} \Phi_J(\boldsymbol{x}) \sum_{\beta=1}^{N_a} \int_{\Omega(\boldsymbol{x}')} \frac{1}{\Delta V(\boldsymbol{x}')} \boldsymbol{F}^{\alpha\beta}[\Phi_I(\boldsymbol{x})\boldsymbol{U}_I^\alpha, \Phi_K(\boldsymbol{x}')\boldsymbol{U}_K^\beta]\, \mathrm{d}\Omega(\boldsymbol{x}')\, \mathrm{d}\Omega(\boldsymbol{x})$$

$$\approx \sum_{I_\mathrm{p}=1}^{N_p} n_{I_p} \sum_{j\in\psi_{I_\mathrm{p}}} \sum_{k=1}^{N_l} \sum_{\beta=1}^{N_a} \Phi_J(\boldsymbol{x}_j) \boldsymbol{F}^{\alpha\beta}[\Phi_I(\boldsymbol{x}_j)\boldsymbol{U}_I^\alpha, \Phi_K(\boldsymbol{x}_k)\boldsymbol{U}_K^\beta], \tag{33}$$

where n_{I_p} is the weight of the I_pth cluster and N_p is the number of all nodes. When the clusters shrink to the size of the rep-cells, i.e. $\psi_{J_\mathrm{p}} = \{J_\mathrm{p}\}$, it holds $\Phi_I(\boldsymbol{x}_{J_\mathrm{p}}) = \delta_{IJ_\mathrm{p}}$, and the cluster summation rule boils down to a node-based summation rule

$$\boldsymbol{F}_J^\alpha = n_J \sum_{k=1}^{N_l} \sum_{\beta=1}^{N_a} \boldsymbol{F}^{\alpha\beta}[\boldsymbol{U}_J^\alpha, \Phi_K(\boldsymbol{x}_k)\boldsymbol{U}_K^\beta]. \tag{34}$$

In this case the weighting factor is n_J, which is the number of unit cells represented by Jth node, thus $n_J = \sum_{j=1}^{N_l} \Phi_J(\boldsymbol{x}_j)$. On the other extreme, $n_J = 1$, implies all pairs of interatomic forces are calculated. In all cases $\sum_{I_\mathrm{p}} \sum_{j\in\psi_{I_\mathrm{p}}} n_{I_\mathrm{p}} = N_l$ holds.

Figure 3 shows the numerical procedures to calculate the interatomic force between any two atoms. The force between any two atoms in different or same unit cells should be distributed to all the nodes of the elements, in which the two unit cells reside. For example, there is a unit cell l located within cluster ψ_p with weighting factor n_p and there is another generic unit cell k; $\{\boldsymbol{f}^{k\alpha}_{l\beta}, \boldsymbol{f}^{l\beta}_{k\alpha}\}$ represents a pair of interatomic forces acting on the $k\alpha$th atom and the $l\beta$th atom, $\boldsymbol{f}^{k\alpha}_{l\beta} = -\boldsymbol{f}^{l\beta}_{k\alpha}$; through shape function $\Phi_{kI} = \Phi_I(\boldsymbol{x}_k)$, force $n_\mathrm{p}\Phi_{kI}\boldsymbol{f}^{k\alpha}_{l\beta}$ is distributed to the αth atom of node I; similarly, $n_\mathrm{p}\Phi_{kJ}\boldsymbol{f}^{k\alpha}_{l\beta}$, $n_p\Phi_{kK}\boldsymbol{f}^{k\alpha}_{l\beta}$ and $n_\mathrm{p}\Phi_{kL}\boldsymbol{f}^{k\alpha}_{l\beta}$ are distributed to the αth atom of nodes J, K and L; in the same way, $n_\mathrm{p}\Phi_{lJ}\boldsymbol{f}^{l\beta}_{k\alpha}$, $n_p\Phi_{lK}\boldsymbol{f}^{l\beta}_{k\alpha}$, $n_\mathrm{p}\Phi_{lG}\boldsymbol{f}^{l\beta}_{k\alpha}$ and $n_\mathrm{p}\Phi_{lH}\boldsymbol{f}^{l\beta}_{k\alpha}$ are distributed to the βth atom of nodes J, K, G and H.

4. Simulation results

In this work, we consider a given electromagnetic wave propagating in a MgO specimen of nanoscale. The ionic MgO crystal (figure 5(*a*)) belongs to $Fm\bar{3}m$ space group, and has cubic structure with lattice constant $a = 0.42\,\mathrm{nm}$. The interatomic potential employed here is the combination of the long range electrostatic Coulomb potential and the short range Buckingham potential with the material parameters listed in table 1 [28]. The Coulomb–Buckingham potentials between pairs of two atoms, Mg–Mg, O–O, Mg–O, are employed as

$$U^{\xi\eta} = \frac{q^\xi q^\eta}{r^{\xi\eta}} + A^{\xi\eta} \exp\left(-\frac{r^{\xi\eta}}{\rho^{\xi\eta}}\right) - \frac{C^{\xi\eta}}{(r^{\xi\eta})^6}, \tag{35}$$

where $A^{\xi\eta}$, $\rho^{\xi\eta}$ and $C^{\xi\eta}$ are material constants; $r^{\xi\eta} \equiv \|\boldsymbol{r}^{\xi\eta}\| \equiv \|\boldsymbol{r}^\xi - \boldsymbol{r}^\eta\|$.

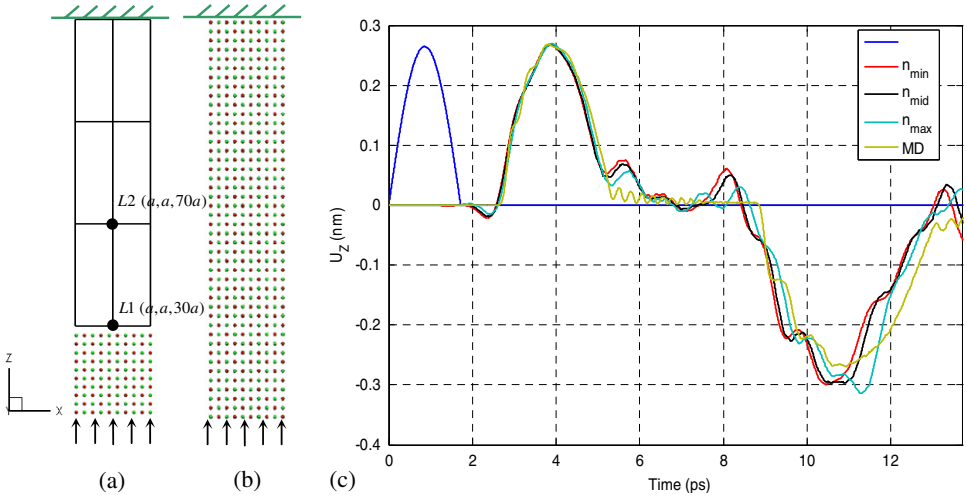

Figure 4. Wave propagation through the interface between the atomic region and the continuum region. The computational model of AFT and MD under a compressive impulsive loading is illustrated in (*a*) and (*b*), respectively. Displacement response of Point $L2$ $(a, a, 70a)$ under the loading with the frequency $\omega \approx 1.6$ THz is shown in (*c*).

In MD simulations or in our AFT method, only interatomic potential is needed for reproducing the lattice parameters [29], elastic constants [30], specific heat, thermal conductivity, thermal expansion, etc.

4.1. Validation

In this subsection, through the simulation of a critical phenomenon in concurrent multiscale modeling [31, 32]—wave propagation across the interface between the atomic region and the continuum region, we have demonstrated the robustness and stability of our numerical methodology using nodal integration. We now briefly summarize the performed simulation here. From figures 4(*a*) and (*b*), it is shown that the 3D molecular dynamical model and the AFT model ($2a \times 2a \times 150a$) of the MgO crystal are subjected to a compressive impulsive loading along the z-direction. It is also noted that the resolution in the z-direction between the atomic region and the continuum region has a dramatic change since the size of element in the continuum region is $1a \times 1a \times 10a$. Figure 4(*c*) shows the responses at point $L2$ $(a, a, 70a)$ (which is located behind the interface $z = 30a$) with three different cluster weighting factors $n_{\min}, n_{\text{mid}}$ and $n_{\max}$ under the compressive impulsive loading with the frequency $\omega \approx 1.6$ THz. Here $n_{\min} = 1$ (cluster having the largest size) represents the simulation with all pairs of interatomic forces calculated; $n_{\max}$ (cluster having the smallest size) represents the simulation with node-based summation rules and n_{mid} ($n_{\min} < n_{\text{mid}} < n_{\max}$) (cluster having a size between the two extreme cases) represents the simulation with general cluster summation rules. In figure 4(*c*), the blue line represents the input impulsive loading along the z-direction. It is clearly seen that the results from AFT are in good agreement with that from MD simulation. Also it is noted that the wave in the AFT model passes through the atomic–continuum interface with negligible reflection. As expected, the results with smaller cluster weighting factor are smoother and closer to those from MD simulation.

With respect to the sensitivity of FE size, we have shown [31] that the interface between meshes with different sizes acts like a screen, which prevents at least part of the wave from

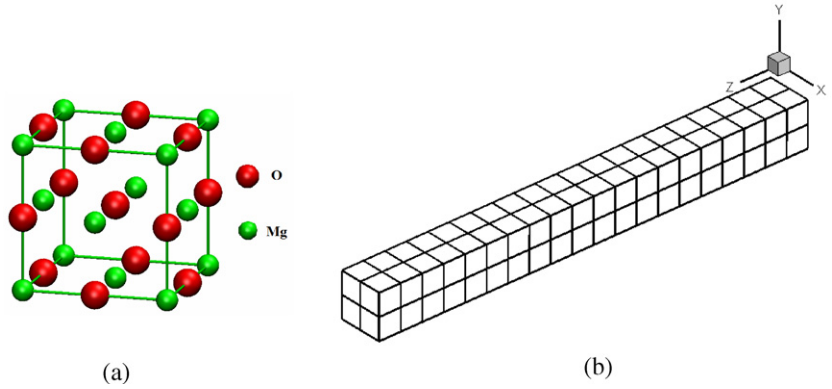

Figure 5. (*a*) Crystal structure of MgO and (*b*) the finite element model of the specimen.

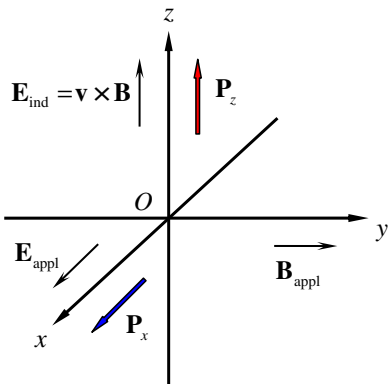

Figure 6. Scheme to illustrate the polarization response subject to an EM wave.

passing through. Actually this is a well-known phenomenon that wave reflection happens when nonuniform mesh is used in the classical FE analysis.

4.2. Effects of electromagnetic wave

In this work, we assume that temperature is at 0 K. A MgO nanowire (1.6 nm × 1.6 nm × 16 nm, 8200 atoms) subject to a given electromagnetic field is modeled with 80 FEs and 189 nodes in figure 5(*b*). The initial displacement and velocity of each node are zero after a long time relaxation; no loading and no boundary constraints are applied in the simulation. The radius of the cluster used in this work is 0.2 nm and the time step is 1 fs. The body force, i.e. the Lorentz forces acting on the charged atoms, is caused solely by the external EM field. The polarization response can be schematically illustrated by figure 6. Driven by the Lorentz force, according to equation (22), the charged ions Mg^{2+} and O^{2-} in the specimen will move along the$x$-direction first with the velocity v_x induced by the applied electric field E_x. This motion gives rise to a polarization P_x. Then due to the motion of ions in the x-direction and the applied magnetic flux density along the y-direction, B_y, a Lorentz force, equal to $q^\alpha \boldsymbol{v} \times \boldsymbol{B}/c$ arises in the z-direction. Hence, the charged ions will move in the z-direction that generates polarization P_z as well.

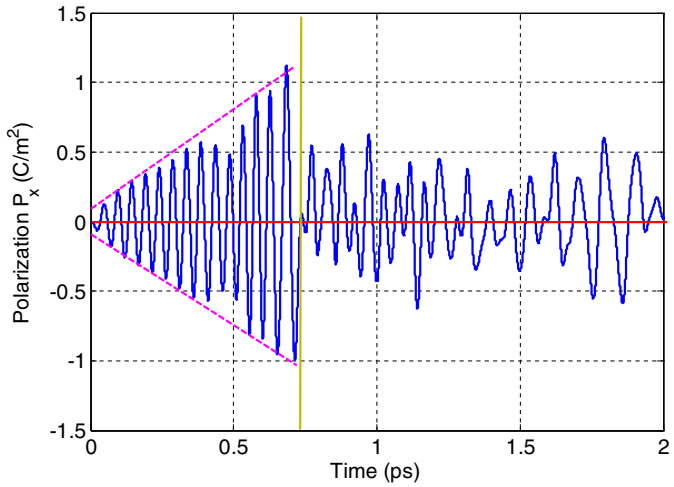

Figure 7. Polarization P_x versus time with frequency $\omega = \omega_{\mathrm{r}} = 130\,\mathrm{THz}$.

First, let Maxwell's equations be expressed in the Heaviside–Lorentz system and let the external EM field satisfy Maxwell's equation under the idealized vacuum situation. Under the Heaviside–Lorentz system, $\boldsymbol{E}$ and $\boldsymbol{B}$ have the same dimension $\mathrm{V\,m^{-1}}$. Also, because we consider the external fields satisfy Maxwell's equations in vacuum, we have $\boldsymbol{B} = \boldsymbol{H}$ and $\boldsymbol{E} = \boldsymbol{D}$. Second, in this work, we only consider one-way coupling, in other words, the external EM wave will induce motions, including polarization $\boldsymbol{P}$, in the crystal; but the crystal will have no effect on the external $\boldsymbol{E}$ and $\boldsymbol{B}$ fields. Here, the harmonic electric field $\boldsymbol{E} = [E_x\ E_y\ E_z] = [E_x\ 0\ 0]$ and magnetic flux density $\boldsymbol{B} = [B_x\ B_y\ B_z] = [0\ B_y\ 0]$with variance in time and space are applied with

$$E_x = B_y = \begin{cases} A\ \exp[\mathrm{i}\omega(z - ct)/c] & \text{if } t \leqslant 10\pi\omega, \\ 0 & \text{if } t > 10\pi\omega, \end{cases} \tag{36}$$

where c is the speed light, $A = 148\,\mu\mathrm{V\,nm^{-1}}$ is the amplitude and ω is the frequency of the EM wave. Here three cases are considered: case I (high frequency) $\omega = \omega_{\mathrm{h}} = 260\,\mathrm{THz}$; case II (resonance frequency) $\omega = \omega_r = 130\mathrm{THz}$; case III (low frequency) $\omega = \omega_{\mathrm{l}} = 26\,\mathrm{THz}$.

At atomic level computations, classically, the polarization $\boldsymbol{P}$ is defined as the dipole moment per unit volume

$$\boldsymbol{P} = \frac{e}{\Delta V} \sum_n Z_n \boldsymbol{R}_n, \tag{37}$$

where $\boldsymbol{R}_n$ is the position vector of charge Z_n, e is the unit of charge and ΔV is the volume of unit cell. Consequently, it is straightforward to show the polarization density $\boldsymbol{P}(\boldsymbol{x}, t)$ of a lattice point in AFT as

$$\boldsymbol{P}(\boldsymbol{x}, t) = \sum_{k=1}^{N_l} \sum_{\alpha=1}^{N_a} q^{k\alpha} (\boldsymbol{R}^k + \Delta \boldsymbol{r}^{k\alpha}) \delta(\boldsymbol{R}^k - \boldsymbol{x}) = \sum_{k=1}^{N_l} \sum_{\alpha=1}^{N_a} q^{k\alpha} \Delta \boldsymbol{r}^{k\alpha} \delta(\boldsymbol{R}^k - \boldsymbol{x}), \tag{38}$$

where $q^{k\alpha}$ is the charge of the $k\alpha$th atom and $\Delta \boldsymbol{r}^{k\alpha}$ is the current relative position of the $k\alpha$th atom with respect to the centroid of unit cell k. Equation (38) can give us both the local and bulk values of the polarization of a finite size specimen.

According to equation (38), the polarization density can be calculated as a vector-valued function of space and time. Figure 7 shows polarization P_x of the x–y cross section at $z = 8\,\mathrm{nm}$

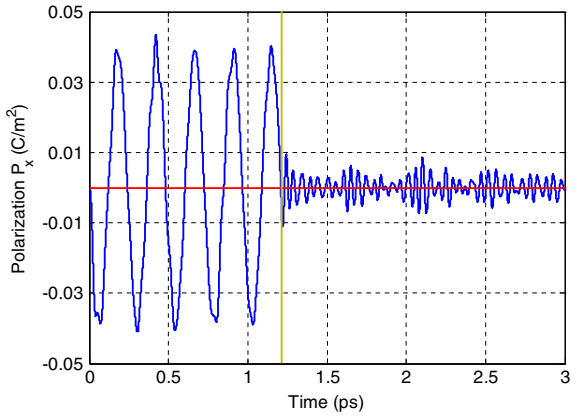

(a) $\omega = \omega_r = 26$THz

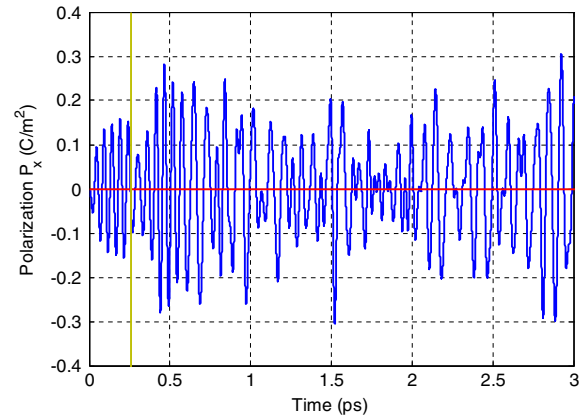

(b) $\omega = \omega_r = 130$THz

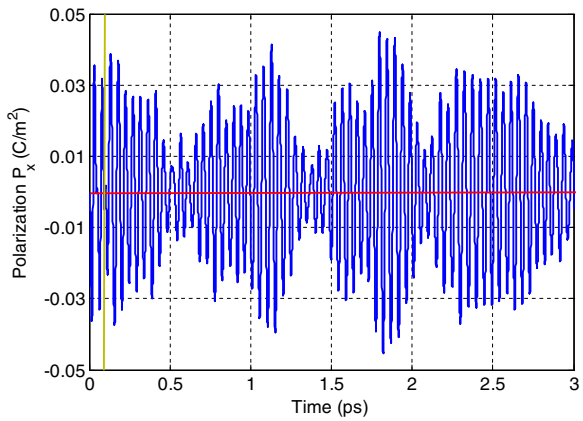

(c) $\omega = \omega_r = 260$THz

Figure 8. Polarization P_x versus time under different frequencies.

with $\omega = 130$ THz. From the pattern of the response, it is noted that this special frequency will drive P_x to a resonance state as we expected in the classical vibration system. Resonance is the tendency of a system to absorb more energy when the driving frequency matches the system's natural frequency. It will cause violent swaying motions and catastrophic failure of the

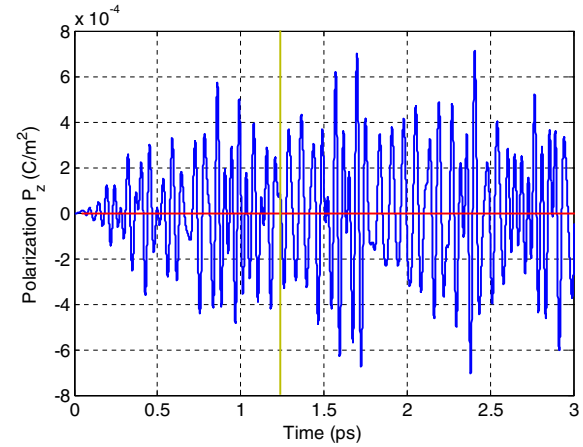

(a) $\omega=\omega_r$ = 26THz

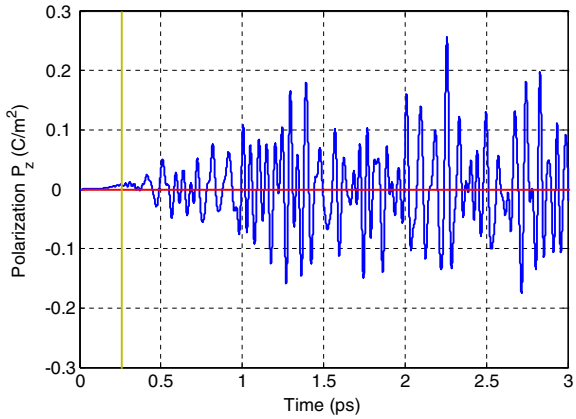

(b) $\omega=\omega_r$ = 130THz

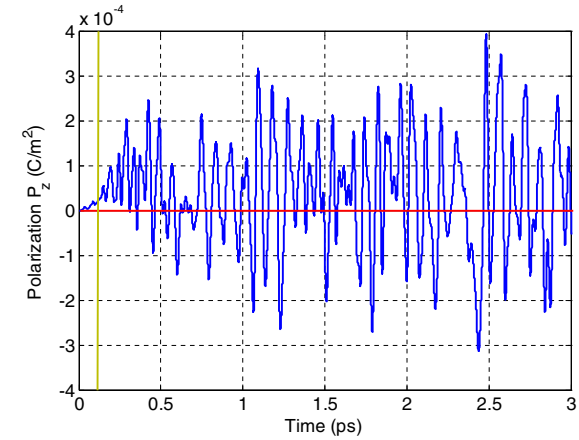

(c) $\omega=\omega_r$ = 260THz

Figure 9. Polarization P_z versus time under different frequencies.

specimen had we not terminated the driving EM wave. That is why we identify $\omega \approx 130$ THz as the resonance frequency.

The polarization components P_x and P_z of the x–y cross section at $z = 8$ nm are plotted as functions of time for case I, II and III in figure 8 and figure 9, respectively. It is noted that in the simulation there are two stages divided at $t = t_a = 10\pi\omega$ (the orange lines in figures); in the second stage, $t > t_a$, the external EM wave is terminated.

When time $t \leqslant t_a$, along the x-direction, figure 8 shows the distinct responses of polarization P_x to the applied EM wave with different driving frequencies. It is observed that the applied high-frequency (low-frequency) electric field E_x drives P_x to a frequency larger (smaller) than the natural frequency. However, the magnitudes of P_x are comparable. It is seen that the magnitude of P_x is much larger at resonance frequency. From figure 9, we can see the response of P_z are delayed under the applied EM wave. This is due to the fact that P_x is caused by E_x directly and, on the other hand, P_z is caused by the joint effect v_x and B_y.

When time $t > t_a$, there is no external field, only the interatomic force exists. Then the effect of the EM wave disappears and the polarization mainly follows its natural frequency of the specimen irrespective of what has been applied $t \leqslant t_a$ (cf figures 8 and 9).

5. Conclusions

Through AFT, the internal deformation of the microstructure in a nano-sized continuum under the influence of an EM wave on the polarizable material MgO is investigated. The major findings of this work are summarized as follows:

(1) AFT is naturally suitable to multi-element crystals because it enables us to find the atomistic trajectories of each atom in the unit cell (cf the superscript α in the governing equation (21)).
(2) As a compromise between efficiency and accuracy, we adopt a cluster-based summation rule for force calculations in the FE formulations. However, our numerical algorithm is a general one: at one extreme, only nodes are representative; at the other extreme, all atoms in the system are self-representative.
(3) In AFT simulations, the majority of degrees of freedom are eliminated and the computation cost is largely reduced. Nevertheless, the essential dynamic, nonlinear, nonlocal, large-deformation material behaviors can be successfully presented.
(4) This work shows that polarization of MgO can be induced by the applied electromagnetic wave. In particular, we demonstrated the resonance phenomenon which occurs when the frequency of the EM wave approaches the natural frequency of the system. This means AFT can be used to analyze the thermomechanical–electromagnetic coupling phenomena of multi-element crystal materials at micro/nanoscale within one theoretical framework.

References

[1] Eringen A C and Suhubi E S 1964 Nonlinear theory of simple micro-elastic solids: I *Int. J. Eng. Sci.* **2** 189–203
[2] Eringen AC and Suhubi E S 1964 Nonlinear theory of simple micro-elastic solids: II *Int. J. Eng. Sci.* **2** 389–404
[3] Eringen A C 1999 *Microcontinuum Field Theories: I. Foundations and Solids* (New York: Springer)
[4] Chen Y P and Lee J D 2004 Determining material constants in micromorphic theory through phonon dispersion relations (vol 41, pg 871, 2003) *Int. J. Eng. Sci.* **42** 1097–7
[5] Zeng X W, Chen Y P and Lee J D 2006 Determining material constants in nonlocal micromorphic theory through phonon dispersion relations *Int. J. Eng. Sci.* **44** 1334–45
[6] AbrahamF F, Broughton, J Q, Bernstein N and Kaxiras E 1998 Spanning the continuum to quantum length scales in a dynamic simulation of brittle fracture *Europhys. Lett.* **44** 783–7

[7] Wagner G J and Liu W K 2003 Coupling of atomistic and continuum simulations using a bridging scale decomposition *J. Comput. Phys.* **190** 249–74
[8] Xiao S P and Belytschko T 2004 A bridging domain method for coupling continua with molecular dynamics *Comput. Methods Appl. Mech. Eng.* **193** 1645–69
[9] Chen W and Fish J 2006 A generalized space-time mathematical homogenization theory for bridging atomistic and continuum scales *Int. J. Numer. Methods Eng.* **67** 253–71
[10] Parks M L, Bochev P B and Lehoucq R B 2008 Connecting atomistic-to-continuum coupling and domain decomposition *Multiscale Modeling Simul.* **7** 362–80
[11] Curtin W A and MillerR E 2003 Atomistic/continuum coupling in computational materials science *Modelling and Simulation in Materials Science Eng.* **11** R33–R68
[12] Miller R E and Tadmor E B 2009 A unified framework and performance benchmark of fourteen multiscale atomistic/continuum coupling methods *Modelling Simul. Mater. Sci. Eng.* **17** 053001
[13] Tadmor E B, Ortiz M and Phillips R 1996 Quasicontinuum analysis of defects in solids *Phil. Mag.* A **73** 1529–63
[14] Irvine J H and Kirkwood J G 1950 The statistical theory of transport processes: IV. The equations of hydrodynamics *J. Chem. Phys.* **18** 817
[15] Hardy R J 1982 Formulas for determining local properties in molecular-dynamics simulations: shock waves *J. Chem. Phys.* **76** 622
[16] Chen Y P 2009 Reformulation of microscopic balance equations for multiscale materials modeling *J. Chem. Phys.* **130** 134706
[17] Chen Y P and Lee J D 2005 Atomistic formulation of a multiscale theory for nano/micro physics *Phil. Mag.* **85** 4095–126
[18] Lee J D, Wang X Q and Chen Y P 2009 Multiscale computation for nano/micromaterials *J. Engrg. Mech.* **135** 192–202
[19] Lee J D, Wang X Q and Chen Y P 2009 Multiscale material modeling and its application to a dynamic crack propagation problem *Theor. Appl. Fract. Mech.* **51** 33–40
[20] Xiong L M and Chen Y P 2009 Coarse-grained simulations of single-crystal silicon *Modelling Simul. Mater. Sci. Eng.* **17** 035002
[21] Chen J, Wang X Q, Wang H C and Lee J D 2010 Multiscale modeling of dynamic crack propagation *Eng. Fract. Mech.* **77** 736–43
[22] Chen Y and Lee J D 2006 Conservation laws at nano/micro scales *J. Mech. Mater. Struct.* **1** 681–704
[23] Cheung K S and Yip S 1991 Atomic-level stress in an inhomogeneous system *J. Appl. Phys.* **70** 5688–90
[24] Dove M T 2005 *Introduction to Lattice Dynamics* (Cambridge: Cambridge University Press)
[25] Jackson J D 1962 *Classical Electrodynamics* (New York: Wiley)
[26] Eidel B and Stukowski A 2009 A variational formulation of the quasicontinuum method based on energy sampling in clusters *J. Mech. Phys. Solids* **57** 87–108
[27] Knap J and Ortiz M 2001 An analysis of the quasicontinuum method *J. Mech. Phys. Solids* **49** 1899–923
[28] Grimes R W 1994 Solution of Mgo, Cao, and TiO_2, in Alpha-Al_2O_3 *J. Am. Ceram. Soc.* **77** 378–84
[29] Lei Y J, Chen Y and Lee J D 2007 Atomistic study of lattice structure of $BiScO_3$ *Comput. Mater. Sci.* **41** 242–6
[30] Xiong L M, Chen Y P and Lee J D 2006 Atomistic measure of the strength of MgO nanorods *Theor. Appl. Fract. Mech.* **46** 202–8
[31] Wang X Q, Lee J D and Deng Q 2010 Modeling and simulation of wave propagation based on atomistic field theory *Trans. ASME, J. Appl. Mech.* **78** 021012
[32] Wang X Q and Lee J D Wave propagating across atomic–continuum interface *Phil. Mag. Lett.* at press